Article

Adsorption of Guanine on Oxygen-Deficient TiO$_2$ Surface: A Combined MD-DFTB/DFT Strategy

Yarkın A. Çetin,* Benjamí Martorell, Francesc Serratosa, and Mònica Calatayud

Cite This: *ACS Omega* 2024, 9, 39043−39050

Read Online

ACCESS | Metrics & More | Article Recommendations | SI Supporting Information

ABSTRACT: Metal oxides (MOs) are key materials in many fields, including technological, industrial, and biomedical applications. In most of these implementations, surface reactivity and reducibility properties are critical considerations. In their nanosized form, MOs exhibit enhanced reactivity that is connected to toxicity. Besides the fact that the biological molecule and the surface of the corresponding material interact chemically, little is known about the toxicological mechanisms involved on the atomic scale. The goal of this study is to investigate the role of TiO$_2$ surfaces in interaction with one genetic base, namely guanine. Using a combination of the quasi-electronic density functional-tight binding molecular dynamics simulations and density functional theory calculations, we explored the adsorption modes of guanine with a stoichiometric and oxygen-deficient anatase TiO$_2$ (101) surface. With such an approach, we have characterized new adsorption modes not previously found, and we have highlighted the relevance of defective surfaces in the adsorption of genetic basis, as a model for explaining possible toxicology mechanisms induced by the adsorption process.
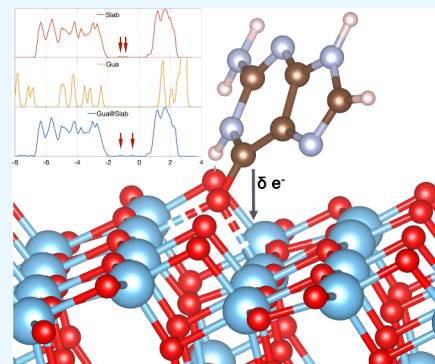
1. INTRODUCTION

Nanoparticles (NPs) have increased their use and importance in the past decade due to their unique properties, but those also give them the potential to be harmful. Recently, it was pointed out that nanosized metal oxide (MO) materials should be less used due to their (nano) toxicity effect, especially in the field of food additives.[1−3] Since it is difficult to foresee the impact it can create, advanced modeling tools may be used for multiscale physics-principled, data-based toxicity assessment via various approaches.[4,5] Therefore, obtaining specific toxicity-pertinent data is important to enlighten the safe use of NPs at a much lower cost than in laboratory and in vivo experiments.

The direct chemical interaction between genetic material and MO surfaces may be a key factor in genotoxic effects. Genotoxicity refers to the harmful changes in DNA that can have significant implications for human health and the environment.[6−16] Given the important role of genetic material in cellular function, extensive research has been conducted on the interactions of common materials used in present technology, for instance, TiO$_2$, which is found in various crystalline forms and exhibits interesting surface properties in today's applications.[17−20] Nevertheless, those properties in TiO$_2$ NPs can harm DNA and cause mutations if not repaired due to their reactive nature.[21,22] Moreover, beyond the direct interaction of TiO$_2$ with genetic bases, titania (a common name for titanium dioxide) may generate reactive oxygen species (ROS), enhanced upon UV light exposure, that are unstable chemicals leading to DNA damage.[23−25] Thus, understanding mechanisms and insights is critical for safer nanomaterials for responsible applications.

Among the different chemical mechanisms for toxicity, the direct nucleotide interactions on the MO surfaces (TiO$_2$, ZnO, CeO$_2$, FeO$_x$, ZrO$_2$, SiO$_2$...), which may modify the chemistry of the nucleotide in the DNA, were explored both experimentally and theoretically by means of the density functional theory (DFT) and density functional-tight binding (DFTB) frames.[26−30] In particular, a DFTB study shows that the cytidine monophosphate nucleotide on the rutile (110) surface favors anchoring with two oxygen atoms by its phosphate side.[31] Another DFT study identifies strong adsorption in guanine-based nucleotides.[32] Nevertheless, a deeper knowledge of the adsorption of single or multiple genetic bases to MO surfaces is required, in particular regarding the role of surface defects, such as oxygen vacancies, which are common in TiO$_2$.[33]
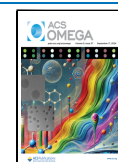
In this work, we aim to explore the effects of TiO$_2$ on genetic basis geometry and electronic structure after adsorption, both for perfect and O-deficient TiO$_2$ surfaces.[26,32,34] Understanding the role of surface defects, such as oxygen vacancies, is important regarding their significance on adsorption characteristics and potential genotoxicity. This may

point to reliable genotoxicity chemical descriptors that can be applied to other nucleotides.[26,32,34]

In the strategy of the present work, we first focused on characterizing the guanine adsorption on a fully oxidized anatase surface from previously reported adsorption modes.[32] Second, we characterized those adsorption modes on O-deficient anatase by means of DFT. Finally, we made a combination of MD-DFTB and DFT to dynamically explore guanine adsorption on both fully oxidized and O-deficient anatases, whose lowest energy structures were then optimized at the DFT level to find novel adsorption modes.

2. COMPUTATIONAL METHODS

2.1. DFTB Molecular Dynamics (MD).
MD simulations were performed in the self-consistent DFTB (SCC-DFTB) framework on the DFTB+ code. DFTB is based on the Taylor expansion and truncation of the electronic structure from DFT calculations, as it is mentioned in detail in.[35−37] These calculations were used to obtain the first description of the adsorption process of guanine on the surface.

The Slater-Koster files are the TIORG ensemble for Ti with O interactions and MIO ensemble for H, C, and N atom interactions. More details on www.dftb.org. Dispersion forces are not considered in the TIORG ensemble.

The convergence criterion through SCC cycles was 10^{-5} eV. Calculations were performed using a spin-polarized electronic optimization procedure. The Nose Hoover thermostat was set in the MD at 300 K, and the Velocity Verlet algorithm for the driver. MD simulations were performed at room temperature to keep molecular and surface structures stable during the dynamics of the simulation, although higher temperatures could accelerate conformational space exploration. Simulation time was 15.000 steps with 1 fs timesteps. All simulations were performed in 3D periodic boundary conditions.

2.2. DFT Calculations.
DFT calculations were performed with the VASP code. VASP computes an approximation to the many-body Schrödinger equation, using either DFT to solve the Kohn−Sham equations or the Hartree−Fock (HF) approximation to solve the Roothaan equations. In VASP, plane-wave basis sets are used to describe the one-electron orbitals.

In this work, we performed calculations in the spin-polarized Perdew−Berke Ernzerhof (PBE) functional.[38] Valence electrons were described on a plane-wave basis set featuring a cutoff of 400 eV. Core electrons were represented using projector-augmented wave (PAW) pseudopotentials.[39,40] The effective Hubbard on-site Coulomb interaction parameter ($U' = U - J = 4$ eV) method was used to describe the behavior of the titanium (Ti) 3d electrons[41] optimized for TiO_2 anatase slab.[42,43] DFT + U is known to provide consistent and reliable results for the electronic structure of TiO_2 and its interactions with organic bases.[38,41] Calculations were performed on the Γ-point. Optimization of the geometry was achieved through the conjugate gradient algorithm. The energy convergence criteria were 10^{-3} eV for the ionic optimization and 10^{-4} eV for the electronic loop. All atoms were allowed to relax. Previously studied slab models in available publications inspired the models that we use in our study for VASP and DFTB+ calculations.[32,42,44,45] Dispersion forces were included via the DFT-D3 method with a Becke-Johnson damping function. Lastly, Bader spin density analysis was performed on optimized structures.[46−49]

2.3. Adsorption Energy.
The adsorption energy of guanine is computed as follows:

$$E_{Ads} = E_{GuaMO_{2n}} - E_{MO_{2n}} - E_{Gua} \qquad (1)$$

$$E_{OVacAds} = E_{GuaMO_{2n-1}} - E_{MO_{2n-1}} - E_{Gua} \qquad (2)$$

E_{Ads} and $E_{OVacAds}$ correspond to the adsorption energy of the models with stoichiometric and oxygen-deficient surfaces, respectively. $E_{GuaMO_{2n}}$ and $E_{GuaMO_{2n-1}}$ defines Gua@Slab models, total energies of slabs are defined by $E_{MO_{2n}}$, and $E_{MO_{2n-1}}$ for stoichiometric and oxygen-deficient models, respectively. Lastly, the energy of a guanine (E_{Gua}) was calculated in a vacuum box of 30 Å.

2.4. Slab Models.
Periodic 3D slabs were created from previous works.[42,44,45] By removing two bottom trilayers of those slabs, we obtained the structure for this study. This was done to take advantage of the computational cost without reducing the coverage scope of the study. The slab model of anatase (101-surface) is displayed in Figure 1A-(101). This
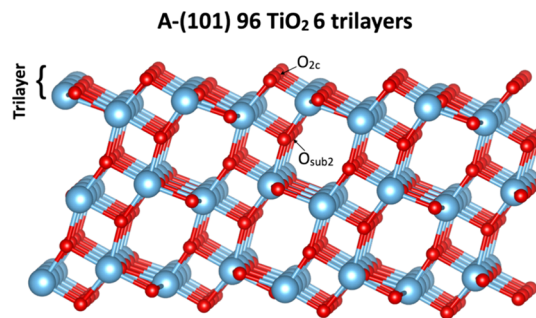

A-(101) 96 TiO₂ 6 trilayers

Figure 1. Side view of the (101) surface organized anatase slab. Ti and O atoms are shown in bright blue and red color, respectively. Oxygen sites are labeled by referring to the oxygen vacancy.

figure also includes oxygen vacancy types.[33] The simulation cell is a (4 × 4) A-(101) surface, which has lattice parameters of $a = 20.63$ Å, $b = 15.48$ Å, and $c = 28.04$ Å. The whole slab structure consisted of 288 (96 Ti, 192 O) atoms (1 atom of the O atom was removed in the O-deficient structures, therefore accounting for 287 atoms in the slab). Single oxygen vacancy creation on the slab structure means 0.52% oxygen deficiency. The oxygen vacancies in this work were O_{2c}-type, as a recent study showed them to be the most stable ones at the DFT level.[33]

To prevent consecutive slabs' interaction in simulations, 18.6 Å of vacuum space was included among consecutive periodic slabs' images in the supercell. This vacuum took into account the genetic base (Gua) in the model to avoid interaction with the mirroring surface since its maximum width is ~7.5 Å.

Adsorption models of guanine on A-(101) were prepared by placing guanine over a slab at a 2 Å distance (see Figure 2 insets), with different rotation angles depending on the adsorption mode. For O-deficient models, the vacancy was accessible to Gua. The complete adsorption model (for no O-vacancy case) consisted of 304 atoms (96 Ti, 193 O, 5 C, 5 N, and 5 H).

3. RESULTS AND DISCUSSION

In this section, we first focused on characterizing the guanine adsorption on fully oxidized (stoichiometric) anatase surfaces
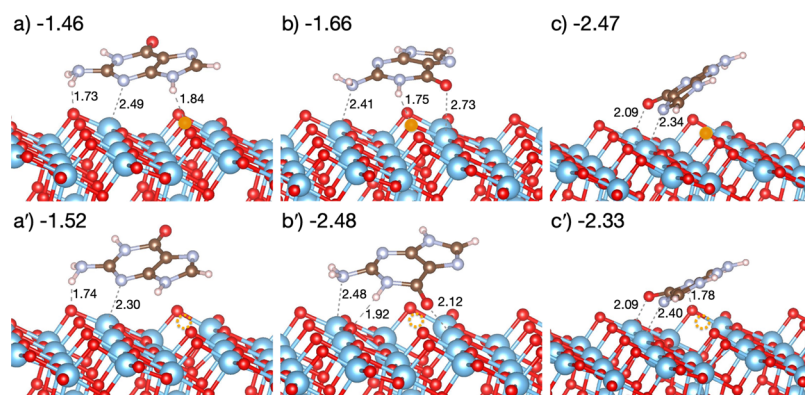
Figure 2. Adsorption modes of guanine on TiO$_2$ (101) together with the adsorption energy in eV (Gua@Slab). The top row is stoichiometric TiO$_2$ (101). The bottom row is the adsorption on an O$_{2c}$-type of O-deficient TiO$_2$ (101). Oxygen vacancy centers are marked with a yellow dashed circle. Distances in Å. Red for O, blue for Ti, brown for C, and gray for N.

from previously reported adsorption modes.[50] As a second step, we characterized those adsorption modes on O-deficient anatase by means of DFT. O-deficient anatase surfaces were previously characterized in our group. The most stable type of OVac was the O$_{2c}$ type (shown in Figure 1) at the DFT level. Finally, we made a combination of MD-DFTB and DFT to reassemble guanine adsorption on both fully oxidized and O-deficient.

3.1. Guanine Adsorption on Stoichiometric TiO$_2$. The initial step in this work was the study of the adsorption modes of guanine on the bare A-TiO$_2$ (101) surface. A previous work by Soria *et* Di Valentin[32] found three main stable adsorption modes for guanine on the same TiO$_2$ surface, shown in Figure 2 (inset a−c). Those calculations were performed with the package CRYSTAL14,[51] making use of periodic boundary conditions with atomic orbitals and B3LYP-D* hybrid DFT functional (Table 1). Note that the most stable adsorption

Table 1. Guanine Adsorption Energies (in eV) on Stoichiometric TiO$_2$ Surface at B3LYP-D*[32] and at GGA + U-D, as well as O-Deficient TiO$_2$ Surface at GGA + U-D

| | | GGA + U-D | |
adsorption mode	B3LYP-D*	stoichiometric	O-deficient
a	−1.45	−1.46	−1.52
b	−1.67	−1.66	−2.48
c	−2.42	−2.47	−2.33

structure (inset) is the only minimum with a direct interaction of the O atom of the guanine and the Ti atom on the surface (2.09 Å). This distance, though longer than the Ti−O bond length in organometallic Ti-based catalysts (around 1.75−1.85 Å[52] in B3LYP), indicates the existence of a clear chemical adsorption interaction.

Our calculations performed at GGA + U-D converged into the same structures obtained by Soria et Di Valentin's (Figure 2, inset a−c). Table 1 shows the adsorption energy levels. Even though the energy adsorption may be affected by the level of the functional used in the DFT calculation, the same values in energy levels as previously reported (a > b > c) was found, within the limits of the DFT accuracy. This correspondence in E_{ads} was also observed in distances of the adsorption modes. Distance changes from reference paper to our computed values (shown in Figure 2) are as follows: (i) for adsorption mode a, the H(Gua)-O(TiO$_2$) contact changes from 1.81 to 1.73 Å, the

N(Gua)-Ti(TiO$_2$) contact goes from 2.53 to 2.49 Å, the H(Gua)-O(TiO$_2$) 1.90 to 1.84 Å; (ii) for adsorption mode b N(Gua)-Ti(TiO$_2$) distance reduces from 2.49 to 2.41 Å, and the H(Gua)-O(TiO$_2$) contact from 1.87 to 1.75 Å; and (iii) for adsorption mode c the O(Gua)-Ti(TiO$_2$) contact keeps the same value of 2.09 Å, and the N(Gua)-Ti(TiO$_2$) contact from 2.47 to 2.34 Å. Thus, it was clearly stated that the interaction modes in the literature were reproduced with good accuracy in terms of energy and adsorption geometry.

3.2. Guanine Adsorption on Oxygen-Deficient TiO$_2$. TiO$_2$ is well-known for its ability to reduce its oxygen content,[53−55] which makes it a candidate with outstanding properties for photochemical applications; however, this feature creates new reactive sites on the surface, which must be explored to properly describe the physicochemical properties of the material. Therefore, we combined the oxygen-deficient site with the adsorption modes of guanine in Figure 2 (insets a−c). Initial structures were constructed from the optimized adsorption mode in Section 3.1, removing the closest oxygen atom (O$_{2c}$-type O$_{Vac}$) under guanine. After that, the structures were optimized by means of energy minimization at the DFT level (Figure 2, insets a′−c′). Our analysis of the modified structures (insets a′−c′ in Figure 3) revealed the impact of oxygen vacancies on the distances between the adsorbate and TiO$_2$ surface. After removing the O$_{2c}$-type from the surface, the trend in energy levels changed from reported (a > b > c) to a′ > c′ > b′, making b′ the most stable adsorption site (Table 1). Interestingly, this change is related to the local interaction of the O atom in guanine with respect to the surface of the O$_{2c}$ vacancy. Distance changes from reproduced modes (a−c) into our computed values in a′−c′ (shown in Figure 2) are as follows: (i) for adsorption mode a′, the H(Gua)-O(TiO$_2$) contact changes from 1.73 to 1.74 Å, the N(Gua)-Ti(TiO$_2$) contact goes from 2.49 to 2.30 Å, and the H(Gua)-O(TiO$_2$) loses contact; (ii) for adsorption mode b′ N(Gua)-Ti(TiO$_2$) distance goes from 2.41 to 2.48 Å, and the H(Gua)-O(TiO$_2$) contact changes to another O atom with from 1.92 Å distance instead 1.75 Å, indicating that O(Gua)-Ti(TiO$_2$) contact goes from 2.73 to 2.12 Å; (iii) for adsorption mode c′, the O(Gua)-Ti(TiO$_2$) contact remains stable at the value of 2.09 Å, and the N(Gua)-Ti(TiO$_2$) contact from 2.34 to 2.40 Å. An additional close approach between the H atom on the benzene ring of Gua and the ring of O(TiO$_2$) occurs at 1.78 Å. Thus, the impact of oxygen vacancies clearly appears in the analysis. Vacancy centers drive
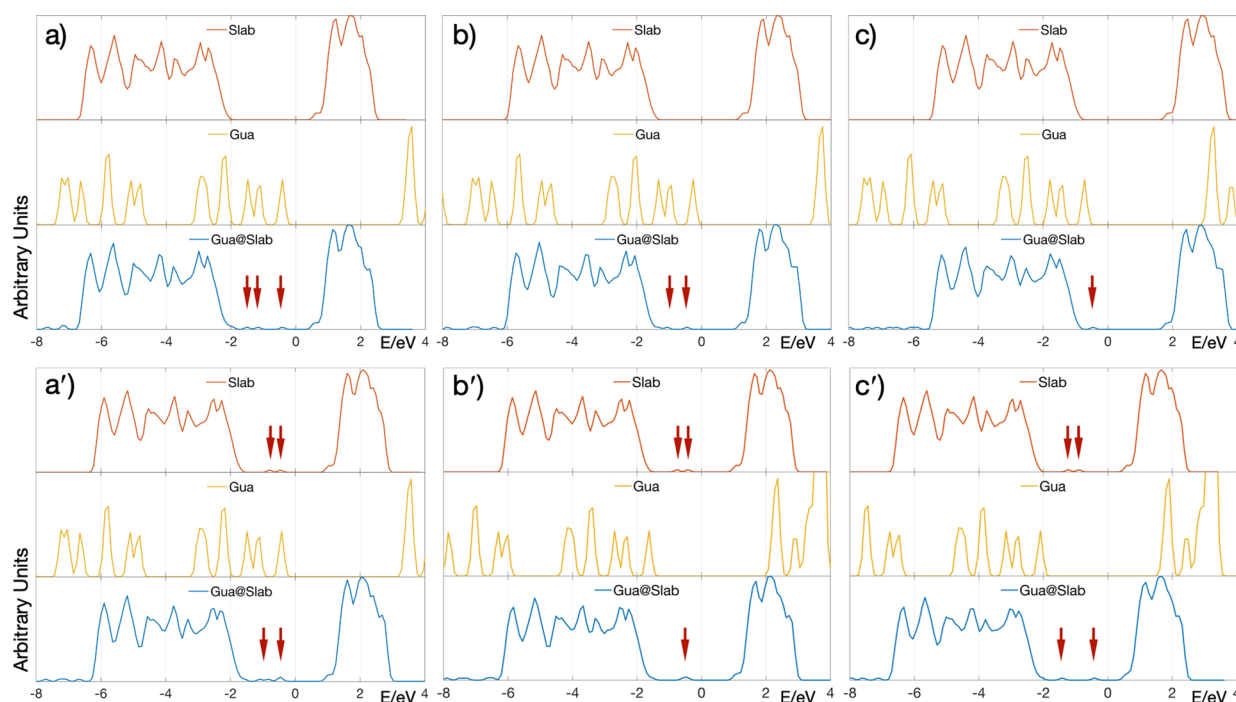
Figure 3. Total density of states (DOS) of each adsorption mode (a, b, c, a′, b′, and c′). Insets follow the same labeling as in Figure 2. For comparison, each inset shows the corresponding slab (orange), guanine (yellow), and Gua@TiO$_2$ mode (blue). Red arrows indicate electron peaks in the band gap. DOS is aligned at the top of the valence band (in orange and blue) for the sake of comparison.

adsorption mode geometries and possible surface contacts. Vacancy models can reveal stronger adsorption modes, as in such change examples in the models a to a′ and b to b′.

In order to analyze the electronic structure of the different adsorption modes of guanine, with and without O vacancies in the TiO$_2$ slab, we plotted the density of states (DOS) of all adsorbed modes (Figure 3). Figure 3 has an analogous layout with insets to Figure 2 in terms of adsorption modes (first row for TiO$_2$ and second row for the O$_{2c}$ vacancy TiO$_2$; each column for an adsorption site). Only the region of valence electron bands and the lowest unoccupied bands are presented.

All DOS plots are aligned with respect to the first noninteracting occupied band of the corresponding Gua@Slab plot. For each adsorption mode, three subinsets are presented: (i) the top row is the TiO$_2$ slab (orange); (ii) the middle layer is guanine (yellow); and (iii) the bottom layer is the adsorbed Gua@TiO$_2$ (blue). Since slab and guanine are common in the adsorption modes, the top and middle rows are equal in all cases and shown for directly comparing changes with the adsorption of guanine.

The bare slab presents a band gap of 2.42 eV; the slab with an O$_{2c}$-type vacancy shows two localized peaks at −1.55 to 0.79 eV in this region (marked with red arrows). A detailed study of this effect is found in a previous work by Çetin et al.[33] A detailed study of the DOS of guanine adsorbed on TiO$_2$ is presented in the Supporting Information (see Figure S1). However, we stress that guanine states fall in the region of the band gap of the slab. This makes that a series of peaks (marked in red) pop up in that region for the adsorbed structures (Figure 3). Those peaks correspond to the interaction of the p-structure of guanine and heteroatom lone pair electrons with the slab. In the case of the O-deficient slab, those interactions also fall in the same region as electrons of the O-vacancy, indicating the possible exchange between guanine and slabs.

3.3. MD for Guanine Adsorption. In order to explore the adsorption of guanine on anatase TiO$_2$ (101) (fully oxidized and with O vacancies) and find new adsorption modes, we made use of MD simulations at room temperature at the DFTB level to find alternative geometries as starting points for DFT optimization. With such a methodology, we may also explore chemical effects present on the surface beyond the adsorption process. Initial structures for MD simulations were those minima from Sections 3.1 and 3.2. Moreover, additional MD simulations with the guanine carbonyl O atom vertically positioned on the O$_{2c}$-type of the slab were made for both fully oxidized and with O-vacancy anatase surface (details of the structure in Supporting Information, Figure S2). We then plotted total energies through the trajectory for 5000 steps. Equilibration was confirmed by ensuring the system's total energy value variations which were within 0.3%. If an MD simulation was not equilibrated, then it was allowed to run up to 15,000 steps. Those single points with the lowest energies in regions of the MD trajectory were then optimized by means of DFT (Supporting Information, Figures S3−S7, Tables S1 and S2).

MD simulations conducted with initial structures of adsorption modes a, b, and c (fully oxidized TiO$_2$ surface) showed that, despite mode c exhibiting the lowest E_{ads}, through the MD run, in comparison to mode a, the model occasionally showcases conformations with relatively higher energies in localized regions, indicating the dynamics of those adsorption modes. Still, conformations within mode c and mode a showed similar energy levels despite the extended trajectory of mode c by an additional 5000 steps. However, none of the adsorption models selected in the MD and optimized afterward showed lower adsorption energy than the reference c adsorption mode. Therefore, as far as we explored the potential surface energy of guanine on TiO$_2$, no other adsorption minima were obtained. Beyond the study of adsorption modes of Gua@TiO$_2$, it was
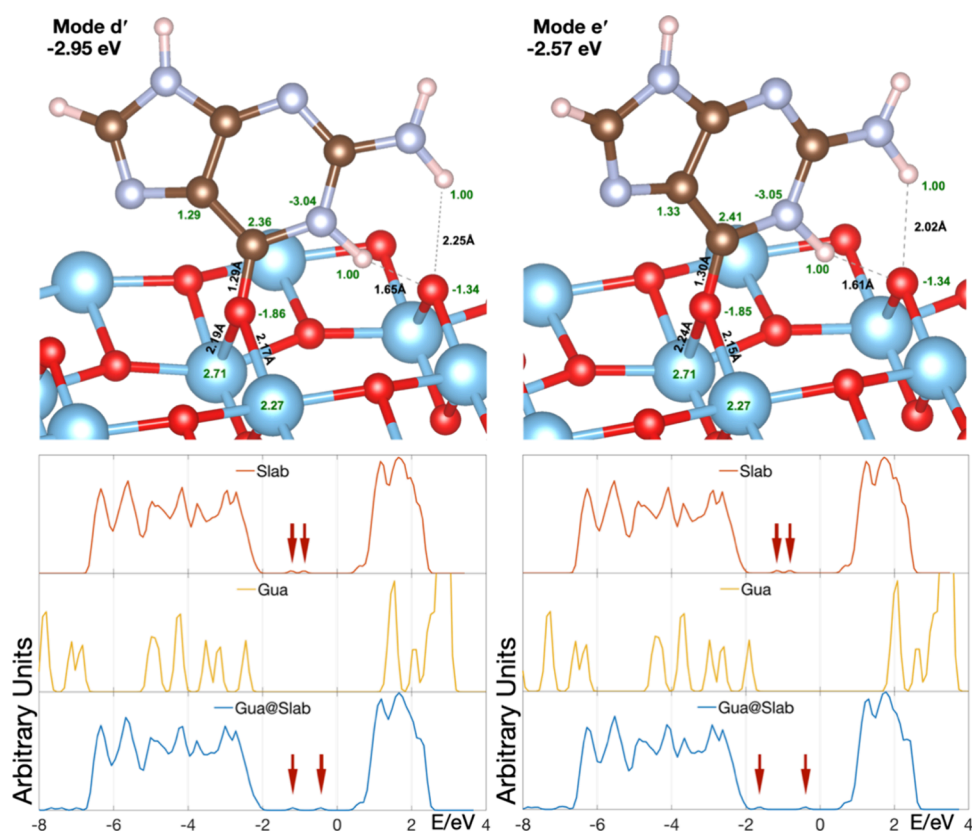
Figure 4. Top rows for adsorption modes d′ and e′ of guanine on O-deficient TiO_2. E_{ads} in eV is in the top left corner of each mode. Distances in Å in black. Bader charges in green for selected atoms. In the bottom row, total density of states (DOS) for each new adsorption mode. Titania slabs are colored orange, guanine yellow, and Gua@TiO_2 in blue. Red arrows indicate electrons in the band gap. DOS plots are aligned to the valence band of Gua@TiO_2.

noteworthy that throughout the MD mode c trajectory, guanine could transfer hydrogen atoms upon interaction with the TiO_2 surface, resulting in configurations where the structural integrity of guanine was compromised in low energy conformations. Though this guanine dehydrogenation catalytically mediated by the surface was not explored in detail, it may indicate a mechanism for the chemical genotoxicity of TiO_2 causing chemical alteration of the genetic basis and the production of ROS, potentially disrupting the genome stability.[25,56] Correspondingly, DNA damage is linked to genotoxicity, which can induce mutations and potential carcinogenicity.[56,57] On the other hand, modes a and b do not exhibit such phenomena.

The next step in this study was performing MD simulations with a TiO_2 slab with the O vacancies. In a previous work, it was observed that DFTB favors the O_{sub2} vacancy type with respect to the O_{2c} type (0.5 eV less stable); in the O_{2c} type, the missing O is directly found on the slab surface, whereas in the O_{sub2}, it locates in the first sublayer.[33] This effect is corroborated in our MD simulations, where the O_{2c} type spontaneously turned into the O_{sub2} vacancy for models only with the O-deficient slab, as well as when the guanine molecule was included in the MD simulation but oriented too far away to interact directly with the O_{2c} vacancy center. We tested the effect of the transformation between O_{2c} and O_{sub2} on total energy stabilization in the model that we use (Supporting Information, Figure S8). Nevertheless, as shown in Section 3.2, the maximum interaction of guanine with the O vacancy was in those cases of an O_{2c} type of vacancy. Therefore, MD

simulations of guanine adsorbed on TiO_2 were restricted to initial structures with an O_{2c} vacancy type (though we performed some MD simulations of guanine on the O_{Sub2} deficient slab modes, none of the structures gave lower adsorption energies at the DFT level than those in previous sections). As described in the methodology, some of the lowest energy snapshots in the trajectory were chosen, and those structure was optimized at DFT level. With such a methodology, two new minima were not found in Section 3.2 arose (Figure 4). The new stable adsorption modes have a direct interaction of the guanine carbonyl O atom filling the O_{2c} vacancy of TiO_2, depicting a strong chemical interaction with the slab. In fact, those two new modes resulted in the lowest E_{ads} structures of the whole study: mode d′ with E_{ads} of −2.95 eV and mode e′ with E_{ads} of −2.57 eV. These energies are 0.47 and 0.09 eV lower with respect to b′ adsorption mode.

Oxygen atoms in the carbonyl group of guanine have two direct bonds to Ti atoms in the slab, with respect to the single interaction in modes a, b, and c. In mode d′, Ti−O, distances are 2.17 and 2.19 Å, whereas for mode e′, distances are 2.15 and 2.24 Å. Also, because of this interaction, the C−O bond in Gua@TiO_2 elongates in these modes. In fact, for guanine in the gas phase, the C−O bond is 1.23 Å, which increases to 1.26 Å for mode c and 1.27 Å for b′, and it rises up to 1.29 and 1.30 Å for mode d′ and mode e′, respectively (see details in Supporting Information, Figure S9). The main difference in the geometry of adsorption mode d′ and mode e′ is the relative tilting angle of guanine with respect to the surface (Figure 4). The distance to the surface of the "tail" part of guanine formed

by the hydrogen atoms of the amino group of guanine is 2.02 Å in mode e′ and 2.25 Å in mode d′. The difference of 0.38 eV in E_{ads} between the two adsorption modes can be associated with the restrictions created by the "tail" in the conformation of the guanine molecule.

The DOS analysis of modes d′ and e′ shows a relative difference in the peaks at −1.2 and −1.8 eV, respectively. Moreover, the Bader charges were computed and analyzed for all adsorption modes (see details in the Supporting Information, Figures S10−S20). The distribution of charges presents minor variations in the key interaction atoms upon adsorption. However, the O atom of the carbonyl group in guanine shows a significant decrease in electron density with respect to different adsorption modes (Table 2). It underscores

Table 2. Bader Charges on the Oxygen of the Carbonyl Group in Guanine (O-Gua) and the Overall Charge Carried by the Guanine Molecule (Gua) for Adsorption Modes on TiO$_2$[a]

adsorption mode	O-(Gua)	Gua
mode a	−1.91	0.07
mode b	−1.90	0.06
mode c	−1.87	0.15
mode a′	−1.92	0.06
mode b′	−1.89	0.06
mode c′	−1.88	0.09
mode d′	−1.86	0.05
mode e′	−1.85	0.02
gas phase	−1.95	0.00

[a]All stoichiometric modes and guanine converge at a singlet spin state, whereas all defective modes converge at a triplet spin state, remaining with two unpaired electrons.

significant shifts in electron density following the same trend as the strength of the adsorption mode, with modes d′ and e′ being the ones with the most significant change transfer from the guanine carbonyl atom to Ti atoms in the surface. Structures of modes d′ and e′ can be found in Supporting Information, Figures S13 and S14. Calculated charges and spin can also be found in the Supporting Information.

4. CONCLUSIONS

In this study, we explored the chemical interaction of guanine on TiO$_2$ in order to determine how adsorption processes on the surface may be a source of genotoxicity descriptors from a modeling point of view. Furthermore, we used a synergistic combination of different levels of calculation (DFT and MD-DFTB) schemes and robustness of first principle calculation in order to speed up the search for adsorption modes of genetic bases on MO surfaces. With such a strategy, we have also analyzed the electronic structure of the systems and the potential stabilization impact on the adsorption modes in more realistic O-deficient TiO$_2$ anatase (101) models.

We studied the adsorption of guanine on stoichiometric and oxygen-deficient anatase TiO$_2$ (101) surfaces to highlight the role of the defects. We found that guanine strongly adsorbs to the stoichiometric TiO$_2$ surface primarily through the electrostatic interaction of the π-electrons parallel to the surface. The presence of oxygen vacancies shifts guanine-TiO$_2$ interaction, leading to enhanced bonding, particularly with guanine's carbonyl oxygen atom occupying the position of the missing oxygen in the TiO$_2$ lattice. In particular, we observed

that there is a charge transfer from the guanine to the slab proportional to the adsorption energy of the adsorption mode.

Our finding of new adsorption modes related to oxygen vacancies on the surface underscores the significance of surface defects, indicating the possibility of new chemistry and genotoxic potential of nanomaterials. Furthermore, MD simulations revealed dynamic aspects of guanine-TiO$_2$ interactions, suggesting surface-induced chemical transformations such as guanine dehydrogenation catalytically mediated by the surface, which may contribute to genotoxic effects. Our findings emphasize the critical role of considering surface defects and dynamics in assessing nanomaterial genotoxicity.

■ ASSOCIATED CONTENT

Data Availability Statement

The research data of this study is available at: https://doi.org/10.34810/data1423.

Ⓢ Supporting Information

The Supporting Information is available free of charge at https://pubs.acs.org/doi/10.1021/acsomega.4c05806.

Detailed DOS analysis; MD simulations; oxygen vacancies' dynamics; and model-related representations (PDF)

■ AUTHOR INFORMATION

Corresponding Author

Yarkın A. Çetin − *Departament d'Enginyeria Informàtica i Matemàtiques, Universitat Rovira i Virgili, 43007 Tarragona, Catalunya, Spain;* ⓞ orcid.org/0000-0003-2456-5949; Email: yarkinaybars.cetin@estudiants.urv.cat

Authors

Benjamí Martorell − *Escola de Doctorat, Universitat Rovira i Virgili, 43002 Tarragona, Catalunya, Spain; Departament d'Enginyeria Química, Universitat Rovira i Virgili, 43007 Tarragona, Catalunya, Spain;* ⓞ orcid.org/0000-0002-7759-8042

Francesc Serratosa − *Departament d'Enginyeria Informàtica i Matemàtiques, Universitat Rovira i Virgili, 43007 Tarragona, Catalunya, Spain;* ⓞ orcid.org/0000-0001-6112-5913

Mònica Calatayud − *CNRS, Laboratoire de Chimie Théorique, LCT, Sorbonne Université, F-75005 Paris, France;* ⓞ orcid.org/0000-0003-0555-8938

Complete contact information is available at:
https://pubs.acs.org/10.1021/acsomega.4c05806

Notes

The authors declare no competing financial interest.

■ REFERENCES

(1) Younes, M.; Aquilina, G.; Castle, L.; Engel, K.; Fowler, P.; Frutos Fernandez, M. J.; et al. Safety assessment of titanium dioxide (E171) as a food additive. *EFSA Journal* 2021, 19, 19.

(2) Blaznik, U.; Krušič, S.; Hribar, M.; Kušar, A.; Žmitek, K.; Pravst, I. Use of Food Additive Titanium Dioxide (E171) before the Introduction of Regulatory Restrictions Due to Concern for Genotoxicity. *Foods* 2021, 10, 1910.

(3) Commission Regulation (EU) 2022/63 of 14 January 2022 amending Annexes II and III to Regulation (EC) No 1333/2008 of the European Parliament and of the Council as regards the food additive titanium dioxide (E 171) C/2022/77. n.d.

(4) Mancardi, G.; Mikolajczyk, A.; Annapoorani, V. K.; Bahl, A.; Blekos, K.; Burk, J.; et al. A computational view on nanomaterial intrinsic and extrinsic features for nanosafety and sustainability. *Mater. Today* 2023, 67, 344.

(5) Çetin, Y. A.; Martorell, B.; Serratosa, F. Prediction of electronic density of states in guanine-TiO2 adsorption model based on machine learning. *Computational and Structural Biotechnology Reports* 2024, 1, No. 100008.

(6) Raja, I. S.; Lee, J. H.; Hong, S. W.; Shin, D. M.; Lee, J. H.; Han, D. W. A critical review on genotoxicity potential of low dimensional nanomaterials. *J. Hazard Mater.* 2021, 409, No. 124915.

(7) Trouiller, B.; Reliene, R.; Westbrook, A.; Solaimani, P.; Schiestl, R. H. Titanium dioxide nanoparticles induce DNA damage and genetic instability in vivo in mice. *Cancer Res.* 2009, 69, 8784−8789.

(8) Chen, H.; Su, S.; Chien, C.; Lin, W.; Yu, S.; Chou, C.; et al. Titanium dioxide nanoparticles induce emphysema-like lung injury in mice. *FASEB J.* 2006, 20, 2393−2395.

(9) De Haar, C.; Hassing, I.; Bol, M.; Bleumink, R.; Pieters, R. Ultrafine but not fine particulate matter causes airway inflammation and allergic airway sensitization to co-administered antigen in mice. *Clin. Exp. Allergy* 2006, 36, 1469−1479.

(10) Grassian, V. H.; O'Shaughnessy, P. T.; Adamcakova-Dodd, A.; Pettibone, J. M.; Thorne, P. S. Inhalation Exposure Study of Titanium Dioxide Nanoparticles with a Primary Particle Size of 2 to 5 nm. *Environ. Health Perspect* 2007, 115, 397.

(11) Oberdorster, G.; Ferin, J.; Lehnert, B. E. Correlation between particle size, in vivo particle persistence, and lung injury. *Environ. Health Perspect* 1994, 102, 173.

(12) Veranth, J. M.; Kaser, E. G.; Veranth, M. M.; Koch, M.; Yost, G. S. Cytokine responses of human lung cells (BEAS-2B) treated with micron-sized and nanoparticles of metal oxides compared to soil dusts. *Part Fibre Toxicol.* 2007, 4, 2.

(13) Federici, G.; Shaw, B. J.; Handy, R. D. Toxicity of titanium dioxide nanoparticles to rainbow trout (Oncorhynchus mykiss): gill injury, oxidative stress, and other physiological effects. *Aquat Toxicol* 2007, 84, 415−430.

(14) Su, J. K.; Byeong, M. K.; Young, J. L.; Hai, W. C. Titanium dioxide nanoparticles trigger p53-mediated damage response in peripheral blood lymphocytes. *Environ. Mol. Mutagen* 2008, 49, 399−405.

(15) Gurr, J. R.; Wang, A. S. S.; Chen, C. H.; Jan, K. Y. Ultrafine titanium dioxide particles in the absence of photoactivation can induce oxidative damage to human bronchial epithelial cells. *Toxicology* 2005, 213, 66−73.

(16) Acar, M. S.; Bulut, Z. B.; Ateş, A.; Nami, B.; Koçak, N.; Yildiz, B. Titanium dioxide nanoparticles induce cytotoxicity and reduce mitotic index in human amniotic fluid-derived cells. *Hum. Exp. Toxicol.* 2015, 34, 74−82.

(17) Bavykin, D. V.; Friedrich, J. M.; Walsh, F. C. Protonated Titanates and TiO2 Nanostructured Materials: Synthesis, Properties, and Applications. *Adv. Mater.* 2006, 18, 2807−2824.

(18) Skipitari, M.; Kalaitzopoulou, E.; Papadea, P.; Varemmenou, A.; Gavriil, V. E.; Sarantopoulou, E.; et al. Titanium dioxide nanoparticle-based hydroxyl and superoxide radical production for oxidative stress biological simulations. *J. Photochem. Photobiol. A Chem.* 2023, 435, No. 114290.

(19) Ayorinde, T.; Sayes, C. M. An updated review of industrially relevant titanium dioxide and its environmental health effects. *Journal of Hazardous Materials Letters* 2023, 4, No. 100085.

(20) Jafari, S.; Mahyad, B.; Hashemzadeh, H.; Janfaza, S.; Gholikhani, T.; Tayebi, L. Biomedical Applications of TiO2 Nanostructures: Recent Advances. *Int. J. Nanomed.* 2020, 15, 3447−3470.

(21) Huang, S.; Chueh, P. J.; Lin, Y. W.; Shih, T. S.; Chuang, S. M. Disturbed mitotic progression and genome segregation are involved in cell transformation mediated by nano-TiO2 long-term exposure. *Toxicol. Appl. Pharmacol.* 2009, 241, 182−194.

(22) Cooke, M. S.; Evans, M. D.; Dizdaroglu, M.; Lunec, J. Oxidative DNA damage: mechanisms, mutation, and disease. *FASEB J.* 2003, 17, 1195−1214.

(23) Petković, J.; Küzma, T.; Rade, K.; Novak, S.; Filipič, M. Pre-irradiation of anatase TiO2 particles with UV enhances their cytotoxic and genotoxic potential in human hepatoma HepG2 cells. *J. Hazard Mater.* 2011, 196, 145−152.

(24) Stone, V.; Johnston, H.; Schins, R. P. F. Development of in vitro systems for nanotoxicology: methodological considerations. *Https://DoiOrg/101080/10408440903120975* 2009, 39, 613.

(25) Armistead, P. M.; Thorp, H. H. Oxidation kinetics of guanine in DNA molecules adsorbed onto indium tin oxide electrodes. *Anal. Chem.* 2001, 73, 558−564.

(26) Mohammadi-Manesh, E.; Mir-Mahdevar, M. Adsorption behavior of guanine, adenine, thymine, and cytosine nucleobases of DNA on zinc oxide-graphene nanosensor: A DFT study. *Synth. Met.* 2020, 267, No. 116486.

(27) Liu, B.; Liu, J. Comprehensive Screen of Metal Oxide Nanoparticles for DNA Adsorption, Fluorescence Quenching, and Anion Discrimination. *ACS Appl. Mater. Interfaces* 2015, 7, 24833−24838.

(28) Liu, B.; Ma, L.; Huang, Z.; Hu, H.; Wu, P.; Liu, J. Janus DNA orthogonal adsorption of graphene oxide and metal oxide nanoparticles enabling stable sensing in serum. *Mater. Horiz* 2018, 5, 65−69.

(29) Limo, M. J.; Sola-Rabada, A.; Boix, E.; Thota, V.; Westcott, Z. C.; Puddu, V.; et al. Interactions between Metal Oxides and Biomolecules: From Fundamental Understanding to Applications. *Chem. Rev.* 2018, 118, 11118−11193.

(30) Cleaves, H. J.; Jonsson, C. M.; Jonsson, C. L.; Sverjensky, D. A.; Hazen, R. M. Adsorption of nucleic acid components on rutile (TiO(2)) surfaces. *Astrobiology* 2010, 10, 311−323.

(31) Gemming, S.; Enyashin, A. N.; Frenzel, J.; Seifert, G. Adsorption of nucleotides on the rutile (110) surface. *Int. J. Mater. Res.* 2010, 101, 758−764.

(32) Soria, F. A.; Di Valentin, C. Binding group of oligonucleotides on TiO2 surfaces: Phosphate anions or nucleobases? *Appl. Surf. Sci.* 2022, 575, No. 151560.

(33) Çetin, Y. A.; Martorell, B.; Serratosa, F.; Aguilera-Porta, N.; Calatayud, M. Analyzing the TiO2 surface reactivity based on oxygen vacancies computed by DFT and DFTB methods. *J. Phys.: Condens. Matter* 2022, 34, No. 314004.

(34) Saha, S.; Sarkar, P. Understanding the interaction of DNA−RNA nucleobases with different ZnO nanomaterials. *Phys. Chem. Chem. Phys.* 2014, 16, 15355−15366.

(35) Elstner, M.; Porezag, D.; Jungnickel, G.; Elsner, J.; Haugk, M.; Frauenheim, T. Self-consistent-charge density-functional tight-binding method for simulations of complex materials properties. *Phys. Rev. B* 1998, 58, 7260.

(36) Koskinen, P.; Mäkinen, V. Density-functional tight-binding for beginners. *Comput. Mater. Sci.* 2009, 47, 237−253.

(37) Seifert, G. Tight-Binding Density Functional Theory: An Approximate Kohn−Sham DFT Scheme†. *J. Phys. Chem. A* 2007, 111, 5609−5613.

(38) Perdew, J. P.; Burke, K.; Ernzerhof, M. Generalized Gradient Approximation Made Simple. *Phys. Rev. Lett.* 1996, 77, 3865−3868.

(39) Kresse, G.; Hafner, J. Ab initio molecular-dynamics simulation of the liquid-metal–amorphous-semiconductor transition in germanium. *Phys. Rev. B* **1994**, *49*, 14251.

(40) Blöchl, P. E. Projector augmented-wave method. *Phys. Rev. B* **1994**, *50*, 17953.

(41) Dudarev, S. L.; Botton, G. A.; Savrasov, S. Y.; Humphreys, C. J.; Sutton, A. P. Electron-energy-loss spectra and the structural stability of nickel oxide: An LSDA U study. *Phys. Rev. B* **1998**, *57*, 1505.

(42) Wei, B.; Calatayud, M. The Subsurface Diffusion of Hydrogen on Rutile TiO2 Surfaces: A Periodic DFT Study. *Top. Catal.* **2021**, *2021*, 270−280.

(43) Wei, B.; Tielens, F.; Calatayud, M. Understanding the Role of Rutile TiO 2 Surface Orientation on Molecular Hydrogen Activation. *Nanomaterials* **2019**, *9*, 1199.

(44) Tielens, F.; Gierada, M.; Handzlik, J.; Calatayud, M. Characterization of amorphous silica based catalysts using DFT computational methods. *Catal. Today* **2020**, *354*, 3−18.

(45) Wei, B.; Calatayud, M. Hydrogen activation on Anatase TiO2: Effect of surface termination. *Catal. Today* **2022**, *397−399*, 113−120.

(46) Yu, M.; Trinkle, D. R. Accurate and efficient algorithm for Bader charge integration. *J. Chem. Phys.* **2011**, *134*, 64111.

(47) Henkelman, G.; Arnaldsson, A.; Jónsson, H. A fast and robust algorithm for Bader decomposition of charge density. *Comput. Mater. Sci.* **2006**, *36*, 354.

(48) Sanville, E.; Kenny, S. D.; Smith, R.; Henkelman, G. Improved Grid-Based Algorithm for Bader Charge Allocation. *J. Comput. Chem.* **2007**, *28*, 899.

(49) Tang, W.; Sanville, E.; Henkelman, G. A grid-based Bader analysis algorithm without lattice bias. *J. Phys: Condens. Matter.* **2009**, *21*, 84204−84211.

(50) Cleaves, H. J.; Jonsson, C. M.; Jonsson, C. L.; Sverjensky, D. A.; Hazen, R. M. Adsorption of Nucleic Acid Components on Rutile (TiO 2) Surfaces. *Astrobiology* **2010**, *10*, 311.

(51) Dovesi, R.; Saunders, V.; Roetti, C.; Orlando, R.; Zicovich-Wilson, C. M.; Pascale, F. et al. *CRYSTAL14 User's Manual*; University of Torino, 2016.

(52) Huang, K. W.; Han, J. H.; Cole, A. P.; Musgrave, C. B.; Waymouth, R. M. Homolysis of weak Ti-O bonds: Experimental and theoretical studies of titanium oxygen bonds derived from stable nitroxyl radicals. *J. Am. Chem. Soc.* **2005**, *127*, 3807−3816.

(53) Rogala, M.; Bihlmayer, G.; Dabrowski, P.; Rodenbücher, C.; Wrana, D.; Krok, F.; et al. Self-reduction of the native TiO2 (110) surface during cooling after thermal annealing − in-operando investigations. *Sci. Rep.* **2019**, *9*, 1−9.

(54) Setvin, M.; Aschauer, U.; Hulva, J.; Simschitz, T.; Daniel, B.; Schmid, M.; et al. Following the Reduction of Oxygen on TiO2 Anatase (101) Step by Step. *J. Am. Chem. Soc.* **2016**, *138*, 9565−9571.

(55) Ganyecz, Á.; Mezei, P. D.; Kállay, M. Oxygen reduction reaction on TiO2 rutile (1 1 0) surface in the presence of bridging hydroxyl groups. *Comput. Theor Chem.* **2019**, *1168*, No. 112607.

(56) Bhattacharya, K.; Davoren, M.; Boertz, J.; Schins, R. P. F.; Hoffmann, E.; Dopp, E. Titanium dioxide nanoparticles induce oxidative stress and DNA-adduct formation but not DNA-breakage in human lung cells. *Part Fibre Toxicol.* **2009**, *6*, 17.

(57) Davanipour, Z.; Poulsen, H. E.; Weimann, A.; Sobel, E. Endogenous melatonin and oxidatively damaged guanine in DNA. *BMC Endocr. Disord.* **2009**, *9*, 22.